Journal of Wind Engineering & Industrial Aerodynamics 273 (2026) 106430

Contents lists available at ScienceDirect

Journal of Wind Engineering & Industrial Aerodynamics

journal homepage: www.elsevier.com/locate/jweia

Evaluation of CFD turbulence models on the aerodynamics of a regional train

Francesco Moro [a,*], Claudio Somaschini [a], Mikel Iraeta [b], Daniele Rocchi [a]

[a] Politecnico di Milano - department of Mechanical Engineering, via Giuseppe La Masa 1, Milan, 20156, Italy
[b] Construcciones y Auxiliar de Ferrocarriles (CAF) - Technology Division. R&D Department, J.M. Iturrioz, 26, Beasain, 20200, Spain

ARTICLE INFO

Keywords:
Regional trains
Train aerodynamics
Drag estimation
CFD models
Turbulence
Wind tunnel

ABSTRACT

The energetic performance of railway vehicles is becoming increasingly important, including for low-speed trains operating on regional and inter-city routes. Aerodynamic drag significantly affects train power consumption, making its accurate estimation essential for the design of energy-efficient rolling stock. Numerical simulations are widely used to estimate aerodynamic resistance; however, simplified fluid-dynamics approaches may lead to inaccurate predictions, particularly for the complex geometries typical of regional trains. This paper compares two numerical methods — Reynolds-Averaged Navier–Stokes (RANS), widely adopted in industry, and the state-of-the-art Improved Delayed Detached-Eddy Simulation (IDDES) — against wind tunnel experiments. Two train geometries are analysed: a conventional regional-train shape and a modified, more streamlined configuration. The analysis focuses on the global aerodynamic drag predicted by the numerical approaches and compares it with experimental measurements. Both methods show satisfactory agreement with the experiments, although noticeable differences emerge. Significant discrepancies are observed in highly turbulent regions, such as the tail, roof, and bogie areas, with IDDES consistently predicting higher drag levels than the RANS model. This work provides new insights into the aerodynamics of regional trains, a vehicle category that has received limited attention so far, and offers results of practical relevance to the railway industry.

1. Introduction

Drag investigation is an important vehicle aerodynamics phenomenon (Baker, 2014a,b; Baker et al., 2019; Sturt et al., 2022). The reason for this is evident: aerodynamic drag is strongly linked to the maximum speed that a vehicle can reach and to the energy consumption that will be required to move it. In the railway field, several techniques can be used to infer the drag force of the vehicles (Baker et al., 2019), even though this process is far from trivial. Experimental methods usually include full-scale testing of the train running resistance and reduced-scale models tested in wind tunnels. Using full-scale tests, the running resistance can be obtained according to the methodology prescribed by the technical norm EN 14067-2:2003 (CEN, 2003) and EN 14067-4:2024 (CEN, 2024) and, from the resulting force, the aerodynamic contribution can be derived by a curve fitting approach, allowing the estimation of the non-dimensional drag coefficient. Wind tunnel tests are widely used to measure forces on portions of simplified train models, modelling various wind conditions. However, these methods come with several drawbacks. The results of full-scale tests are limited to the environmental conditions in which the tests are held and they are available only when the product is already manufactured, meaning that they cannot be used for design decisions. Reduced-scale tests, on the other hand, allow very consistent and repetitive flow conditions reproducing a variety of situations, but present differences from full-scale real conditions. For example, the wind profile close to the ground is hard to model and greatly affects the air flow under the body, which has a very important influence on the overall aerodynamic drag of the vehicle. Wind tunnels usually implement a set of actions to minimise the effect of these issues. In addition, scale effects impact the results, and some differences with reality must be acknowledged (Baker and Brockie, 1991; Tschepe et al., 2021; Li et al., 2022).

An alternative to experimental tests is represented by numerical simulations. With the increasing computational power of the last decades, computational fluid dynamics (CFD) simulations have become more and more accessible (Kisielewicz and Tabbal, 1993; Hemida, 2023; Moukalled et al., 2016). Numerical methods in this context have a very important role as manufacturers' design decisions are supported, other than previous or ad hoc experimental tests, on virtual simulations. CFD tools are mainly used with simplified models such as Reynolds-averaged Navier–Stokes equations (RANS) (Moukalled et al., 2016). Although these methods provide valuable insights, the results could be susceptible to non-negligible errors. Several studies highlight how RANS methods fail to estimate the flow behaviour of bluff

* Corresponding author.
E-mail address: francesco.moro@polimi.it (F. Moro).

https://doi.org/10.1016/j.jweia.2026.106430
Received 18 December 2025; Received in revised form 9 February 2026; Accepted 22 March 2026
Available online 24 March 2026

bodies (Maleki et al., 2017; Zhang et al., 2022, 2023; Guilmineau et al., 2018). To overcome the limitations of RANS methods and, at the same time, to save computational costs from the very precise, yet highly expensive large eddies simulation methods (LES), hybrid RANS-LES (Moukalled et al., 2016) have been developed through the years. From detached eddy simulations (DES) (Spalart et al., 1997; Spalart, 2009, 2021) to its improved versions (DDES Spalart et al., 2006 and IDDES Shur et al., 2008), these models switch from RANS to LES in specific cells allowing for reduced computational effort and better capture flow structures, providing a trade-off in terms of computational cost and results accuracy between the two methods. These models find their application in many industrial fields (Fujita and Sasaki, 2010; Gritskevich et al., 2012; Heinz, 2020), including the railway sector (Luo et al., 2020; Morden et al., 2015; Li et al., 2018; Flynn et al., 2014; Wang et al., 2017). In the railway industrial applications, RANS methods are widely used, as LES and hybrid approaches can be prohibitively expensive in terms of computational cost. However, manufacturing companies often require accurate information on the aerodynamic behaviour of their products. The comparison between a RANS model — representative of typical industrial practice — and a hybrid RANS–LES approach — representative of state-of-the-art research — aims to assess the differences in aerodynamic drag prediction when using a simplified versus a more advanced modelling strategy.

Trains come under different geometries depending on their main purpose. High-speed trains are studied to be as streamlined as possible, facing high manufacturing and maintenance costs to withstand the aerodynamic loads. On the other hand, regional trains must be less expensive and use all the space available to carry high volumes of people and goods. Less strict requirements, motivated by the operational conditions, on regional trains lead to shorter noses and tails, and uncovered equipment on the roof or under the car belly, inevitably worsening the aerodynamic characteristics. These shapes are generally harder to model using simplified CFD models such as RANS, possibly increasing the risk of wrong drag estimation.

While high-speed trains have been extensively investigated in the literature, regional trains remain poorly documented, leaving a clear gap in existing studies. Aerodynamic phenomena can differ significantly between the streamlined shapes of high-speed trains and the generally bluff geometries of regional rolling stock. As a consequence, conclusions drawn for high-speed trains cannot be directly extended to regional trains. The objective of this work is therefore to evaluate and compare the predictions of the two numerical approaches for this specific vehicle type, with particular focus on aerodynamic drag.

Although most of the research in this field is focused on high-speed trains (Brockie and Baker, 1990; Muñoz-Paniagua and García, 2020; Chen et al., 2019; Wang et al., 2021; Yao et al., 2016; Niu et al., 2018; Guo et al., 2022; Wang et al., 2019, 2020; Zhang et al., 2018; Gao et al., 2019; Li et al., 2022, 2019; Huo et al., 2021; He et al., 2022; Yang et al., 2024; Zhao et al., 2026), the aerodynamic drag of regional trains has a relevant impact too. In fact, considering the large number of regional vehicles, reducing their aerodynamic drag would lead to huge energy savings, leading rail transport to be even more sustainable than nowadays (Alšauskas et al., 2023; IEA, 2019; Orellano and Sperling, 2009).

The objective of this research is to evaluate the differences in estimating the drag of regional trains using simple RANS methods against state-of-the-art method IDDES. The evaluation of the results of the numerical simulations is compared against wind tunnel measurements. Two models of trains are considered, presenting two extreme configurations to represent a classical regional train geometry and a high-speed train-like geometry. This research will provide insights on the relative assessment between the two vehicles and the two turbulence modelling methods that have been used.

2. Method

This research relies on a combination of numerical and experimental data to ensure a full-frame evaluation of aerodynamic drag performance of the models studied. Wind tunnel data will be used as a reference for the correlation of the numerical simulations performed. However, the detailed study of CFD is the main target of the present analysis.

This study focuses on a scaled model of a regional train, which consists of two main cars (car A and car B) and a truncated segment of a third car at the tail, referred to as the dummy car. Two distinct configurations of the train are being analysed in this research. The first configuration, named as version 1 (V1), is illustrated in Fig. 1(a) and Fig. 2a. This version represents a traditional regional train design, characterised by the placement of auxiliary equipment on the roof of the cars.

The roof-mounted auxiliary equipment defines this geometry as "rough". The roughness of this version is quantified as the ratio between the typical height of the roof-mounted objects (h) and the boundary-layer height on the roof of the train at the end of the first car (δ), resulting in a value of approximately $h/\delta \approx 35\%$. The second configuration, identified as version 2 (V2), is depicted in Fig. 1(b) and Fig. 2b. In this version, the first car (car A) has been significantly redesigned to mimic the aerodynamic profile of a high-speed train, while the remaining parts of the train retain the same configuration as V1. The car A of this geometry is referred to as "smooth", as no objects protrude from the main frontal area of the train, yielding $h/\delta = 0$.

The selection of these two configurations is driven by the aim of exploring how different numerical methods perform when applied to trains with markedly contrasting geometries, especially concerning the head and tail cars. The model used in this study is scaled to 1:18 of the full-size train, a reduction that ensures quite a fine representation of the geometric details of the design.

Due to the train's asymmetry along its longitudinal axis, both experimental tests and numerical simulations are conducted at two specific yaw angles: 0 degrees and 180 degrees, as illustrated in Fig. 2. When the model is oriented such that car A faces directly into the wind, car A functions as the head car of the train. Conversely, when car A is positioned downstream (180° configuration), it assumes the role of the tail car. This approach allows for the derivation of data that can approximate the behaviour of a theoretically symmetric train, enabling a broader understanding of the aerodynamic characteristics under varying conditions.

2.1. Experimental measurements

Experimental measurements are obtained from a wind tunnel campaign at Politecnico di Milano. The train models are tested at 50 m/s, resulting in a Reynolds number around $Re \approx 6 \cdot 10^5$. The models are placed on a splitter plate with a fixed or non-moving ground. The splitter plate allows a reduction of the thickness of the boundary layer, however, it has to be acknowledged the lack of suction mechanisms or moving ground to actively control its thickness. This implies that parts of the vehicle could be immersed into the ground boundary layer, although its influence should not be large on a 3-car configuration as the one studied. Moreover, the train models are designed to be placed on a single-track ballast and rail. Among the three cars of which the train models are composed, cars A and B are instrumented with internal balances for aerospace applications. The three bodies are not connected one to each other, therefore force and moment measurements are acquired independently and they are representative of every single car. The table on which the model is mounted can rotate, imposing a yaw angle with respect to the wind direction. The tests consist in blowing air at a steady fixed velocity, and acquiring the signals of force and moment for a sufficiently long time in order to extinguish any transient phenomenon. The mean values of the experimental data are derived by

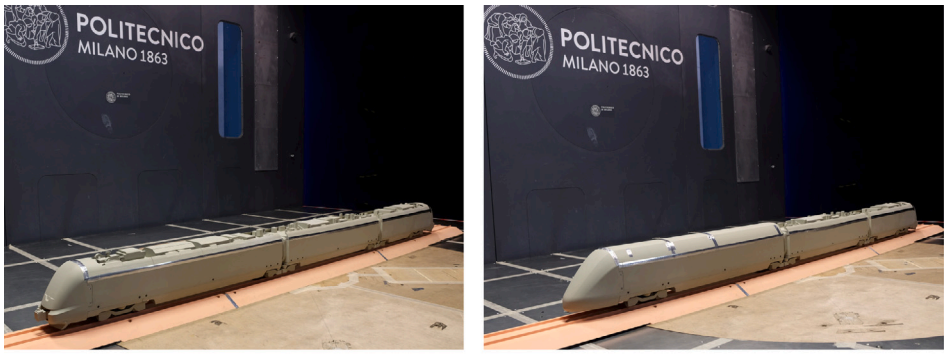

(a) Train V1 (b) Train V2

Fig. 1. Train models tested in the wind tunnel.

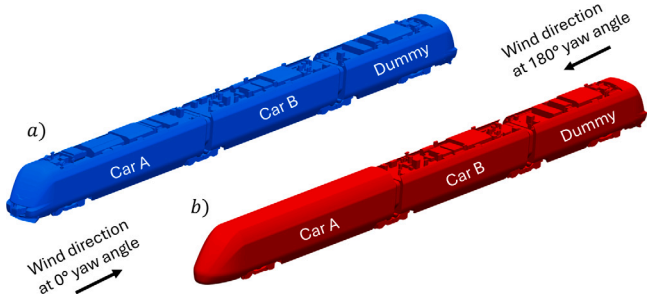

Fig. 2. Versions of train models. (*a*) train version V1. (*b*) train version V2.

averaging the time histories of the signals. The experimental standard error is obtained from the standard measurement error declared by the balance manufacturer. The uncertainty related to the measurement-chain can be attributed around 5% of the measured values. However, it must be acknowledged the possibly larger uncertainty in the estimation of the Car B drag coefficient, as it is a vehicle that experience lower forces and therefore higher relative errors. From the force and moment measurements of the individual cars, the aerodynamic coefficients are derived. For the specific interest of this activity, only the aerodynamic drag is considered, as defined in Eq. (1), with A the reference area, ρ the air density, v the reference speed and C_x the aerodynamic force coefficient in the x direction (corresponding to the drag coefficient).

$$F_{x,aero} = \frac{1}{2}\rho C_x A v^2 \tag{1}$$

2.2. Numerical simulations

Computational fluid dynamics (CFD) simulations for this study are conducted using OpenFOAM, a widely utilised open-source software framework for solving fluid mechanics problems. The simulations consider two distinct CFD modelling approaches: the *Reynolds-averaged Navier–Stokes* (RANS) method and the hybrid RANS-LES approach, specifically the *improved delayed detached eddy simulation* (IDDES) model. These methods are chosen to evaluate their performance and applicability in modelling the aerodynamic behaviour of the train configurations under investigation.

The RANS simulations assume steady-state conditions and employ the $k-\omega$ SST turbulence model, a robust and widely accepted model for various engineering applications. This approach is particularly suitable for capturing steady phenomena, as it resolves the Reynolds-averaged equations, in which turbulence is fully modelled. Consequently, only mean values can be derived from the simulation results. While the aerodynamic behaviour of bluff bodies, such as trains, is inherently unsteady, it is common practice to use RANS simulations under the assumption that the averaged results remain unaffected by transient turbulent fluctuations. This simplification offers a pragmatic approach, particularly in cases where computational efficiency and implementation ease are prioritised.

The hybrid RANS-LES model employed in this study, IDDES, represents a more advanced approach. It integrates RANS modelling (in its unsteady formulation) in regions close to walls, where turbulence is often highly complex and transitions to LES (large eddy simulation) in other areas of the computational domain. Unlike RANS, the LES approach resolves the turbulent structures within the flow up to the level permitted by the spatial resolution of the computational grid. As a result, the turbulence is not entirely modelled but partially resolved, providing a more detailed representation of the flow dynamics.

Previous studies suggest that RANS methods may underestimate the drag force acting on bluff bodies due to their intrinsic limitations in capturing unsteady turbulent phenomena (Maleki et al., 2017; Zhang et al., 2022, 2023; Guilmineau et al., 2018). To address this, the current research aims to simulate the same physical scenario using both modelling approaches. The RANS method, despite its limitations, offers significant advantages in terms of computational speed and ease of implementation, making it particularly appealing for industrial applications. Conversely, the IDDES method, while computationally more demanding, is commonly adopted in academic research for its ability to deliver higher accuracy and capture intricate flow features that are beyond the scope of RANS models.

The simulation scenario under consideration is designed to replicate the conditions of a wind tunnel environment as closely as possible. A simplified schematic representation of this scenario is provided in Fig. 3, where the test section of the wind tunnel serves as the basis for defining the dimensions of the computational domain. To ensure consistency and reliability, the train model geometry and the computational domain size are maintained identical to those utilised in the corresponding wind tunnel experiments. This alignment facilitates direct comparisons between numerical and experimental results.

The outer boundaries of the computational domain are treated as *slip walls*, a boundary condition that assumes no shear stress at the surface. This choice is justified by the low blockage ratio of the setup and the relatively large distance between the train model and the domain walls. Such conditions effectively minimise any significant interaction between the model and the domain boundaries, making this assumption reasonable and ensuring that it does not compromise the accuracy of the simulations.

The only wall with a no-slip boundary condition is located beneath the model, corresponding to the splitter plate. This adherence condition accurately represents the physical setup of the wind tunnel, where the splitter plate serves to minimise ground effects and maintain a consistent flow regime around the train model.

At the domain's inlet, the inflow condition is prescribed as a uniform velocity profile, with a constant velocity magnitude applied across the

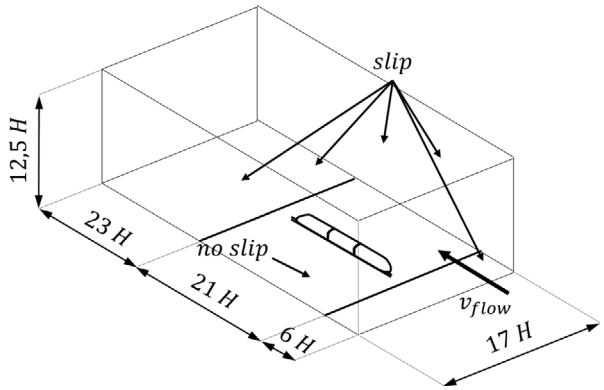

Fig. 3. Scheme of the CFD domain modelling wind tunnel conditions.

Table 1
Grid independence analysis on C_x.

	Coarse mesh	Medium mesh	Fine mesh
Number of cells	$9.5 \cdot 10^6$	$19.2 \cdot 10^6$	$43.4 \cdot 10^6$
ΔC_x%	−0.9%	−0.7%	reference

entire inlet face. This simplification provides a steady and predictable inflow, aligning with the controlled conditions typical of wind tunnel testing. Despite these simplifications, they are deemed sufficiently accurate and representative of the real wind tunnel test environment, as they capture the essential flow characteristics while maintaining computational efficiency.

Before performing the final simulations, the computational grid is evaluated through preliminary RANS simulations to ensure that the results are independent of the grid properties. To achieve this, three different grids are tested: coarse, medium, and fine. The parameter selected for comparison is the overall aerodynamic drag of the train model V1 at a yaw angle of 0°. Using the fine mesh as a reference, the results obtained with the coarse and medium meshes show a very close agreement with those from the fine mesh (Table 1). Based on this comparison, the medium mesh is deemed the optimal choice, offering a compromise between computational efficiency and result accuracy.

The properties of the selected mesh for the simulations and a zoomed-in view of the mesh for the train V1 configuration are presented in Fig. 4, highlighting the refinement level and the attention to detail in critical areas. For the simulations involving the train V2 model and the 180° yaw angle configurations, the mesh is rebuilt while maintaining the same fundamental characteristics to ensure consistency across the cases.

The same computational mesh is employed for both the RANS and IDDES simulations. For the IDDES approach, approximately 80% of the computational domain is resolved using the LES methodology, enabling a detailed representation of turbulence in regions where it is most relevant, while preserving computational feasibility. A dedicated grid-independence study was not performed due to the high computational cost associated with the simulations. Nevertheless, the selected mesh is highly refined and satisfies the requirements typically recommended for hybrid RANS–LES approaches (Pope, 2000; Spalart, 2001). Although no systematic comparison across multiple grid resolutions was carried out, the mesh ensures at least 8–10 cells per integral length scale and is therefore considered adequate to provide reliable predictions for the present application.

3. Results and discussion

The following section covers the following two topics:

Table 2
Relative error comparison between numerical results and wind tunnel experiments.

e_{rel} %		0 deg		180 deg	
		Car A	Car B	Car A	Car B
V1	RANS	−4	−26	−31	−16
	IDDES	10	9	−4	18
V2	RANS	36	−7	−16	−14
	IDDES	33	9	−7	28

- Correlation between experimental (wind tunnel tests) and numerical (CFD simulations) results
- Relative comparison of different approaches within the performed CFD simulations

Wind tunnel tests represent a useful reference for the analysis and correlation of the CFD simulations. However, it is worth mentioning that the main goal of the wind tunnel test campaign was not the assessment of aerodynamic drag but the computation of the aerodynamic coefficients for crosswind stability. This implies a suboptimal arrangement for the assessment of the aerodynamic drag such as a fix ground and a vehicle partially immersed inside the boundary layer. This does not mean correlation with CFD simulations should be negatively affected (same test boundary conditions have been considered) but it is worth noting the uncertainty on the determination of the aerodynamic drag will be higher than for an optimised test setup.

Performed CFD simulations use RANS and IDDES (transient) methodologies to calculate the aerodynamic drag for different vehicle configurations. Obtained results show differences between them. Features like how the roughness affects the boundary layer or how the wake structure on the tail affects the aerodynamic drag are not equally captured by both methodologies. The analysis of these differences provides a deeper insight to understand their limitations and to choose the right option to achieve the defined set of objectives.

The first result involves a direct comparison between the outcomes of wind tunnel tests and numerical simulations, specifically RANS and IDDES, based on the aerodynamic drag coefficient. This comparison is depicted in Fig. 5. To normalise the data and highlight discrepancies, all the results are divided by the experimental mean value of car A ($C_x/C_x|_{WT,A}$). This approach allows for a straightforward assessment of the deviation between the numerical and experimental results for car A, while also enabling indirect comparisons for car B and the dummy car. The coloured region in the plot indicates the absence of experimental data for specific cases; however, numerical results for the dummy car are included for the sake of completeness. The results are reported using the mean value of the coefficients obtained from both the wind tunnel measurements and the numerical simulations. In the latter case, although RANS simulations are intrinsically steady, small numerical oscillations are typically observed around the converged solution. Averaging the sampled values therefore provides a more reliable estimate of the final coefficient.

To ease the validation of the numerical results compared to the experimental data, the relative error e_{rel} is introduced as a metric for the simulation results assessment. The relative error is defined as in Eq. (2).

$$e_{rel} = \frac{C_x|_{num} - C_x|_{WT}}{C_x|_{WT}} \tag{2}$$

The relative error is reported for each simulation in Table 2.

For train V1 at 0 degrees (Fig. 5(a) and top-left area of Table 2), the RANS simulation aligns closely with the experimental results for car A, providing a satisfactory match. In contrast, the IDDES result is less consistent with the experimental value, even though the relative error can be considered still in the uncertainty range of the experimental and numerical estimations. For car B, RANS tends to underestimate the C_x

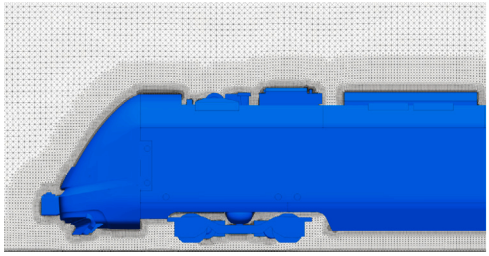

Mesh parameters	Values
Number of cells	$19.2 \cdot 10^6$
Max cell size	70 mm
Min cell size	1 mm
First layer height	0.5 mm
Layers coverage	90 %
Average y^+	30
Wall treatment	wall functions

Fig. 4. Detail of the computational grid and zoomed view close to the head of the train model.

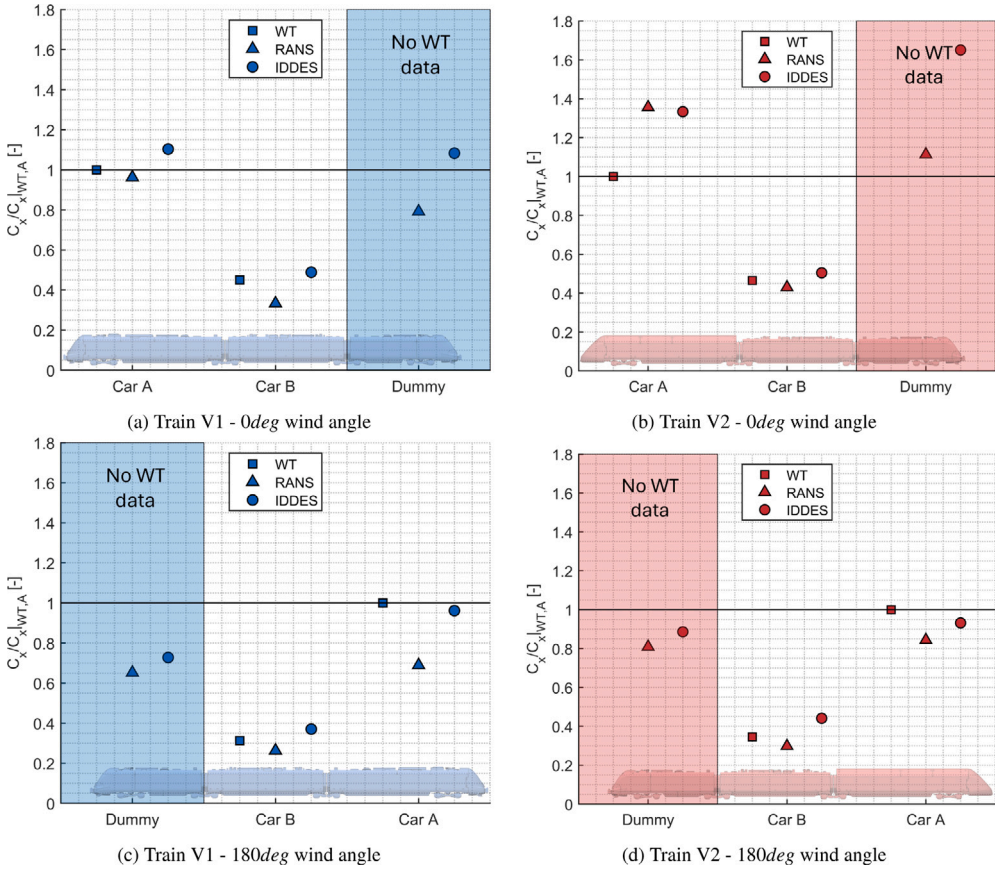

(a) Train V1 - 0*deg* wind angle

(b) Train V2 - 0*deg* wind angle

(c) Train V1 - 180*deg* wind angle

(d) Train V2 - 180*deg* wind angle

Fig. 5. C_x normalised over the wind tunnel value of car A. Comparison between wind tunnel results, RANS and IDDES simulations.

value, whereas IDDES slightly overestimates it. On the dummy body, the results diverge significantly depending on the numerical method used, indicating a pronounced sensitivity to the simulation approach.

In the case of train V2 at 0 degrees (Fig. 5(b) and bottom-left area of Table 2), the results for car A exhibit a notable deviation from the experimental data, regardless of the simulation method applied. For car B, both methods produce results that are closely aligned with the experimental outcomes. However, for the dummy car, the numerical results again show considerable variation between the RANS and IDDES methods.

For the 180-degree configurations, where car A is positioned at the tail of the train model, the results have different outcomes compared to the 0-degree configurations. For train V1 (Fig. 5(c) and top-right area of Table 2), IDDES provides a significantly better match for car A, whereas RANS underestimates the aerodynamic coefficient substantially. For car B, both numerical models show substantial deviations from the experimental data, even though the large error could be attributed to the small value of Car A that amplifies the difference, and on the small value of C_x for car B that may be affected by relatively large uncertainties. On the dummy car, which is now at the head of the train, both methods produce nearly identical results.

For train V2 in the 180-degree configuration (Fig. 5(d) and bottom-right area of Table 2), car A is better captured by the IDDES simulation, though both methods yield comparable results with experimental data. For car B, however, RANS is closer to the experimental data than IDDES, even though the same analysis for V1 at 180-degrees is applicable.

Overall, RANS generally produces lower C_x values compared to IDDES, a trend that becomes more evident for bodies with high geometric roughness (as in train V1) and in cases where the wake of the body is fully developed, such as downwind for car A in the 180-degree configuration or the dummy car in the 0-degree configuration. For tail cars, IDDES emerges as the more accurate model when compared to experimental data, while for the head and middle cars, both numerical methods demonstrate similar levels of performance.

To further clarify the physical origin of the differences between the two modelling approaches, it is useful to distinguish between wake behaviour and near-wall flow features induced by geometric complexity.

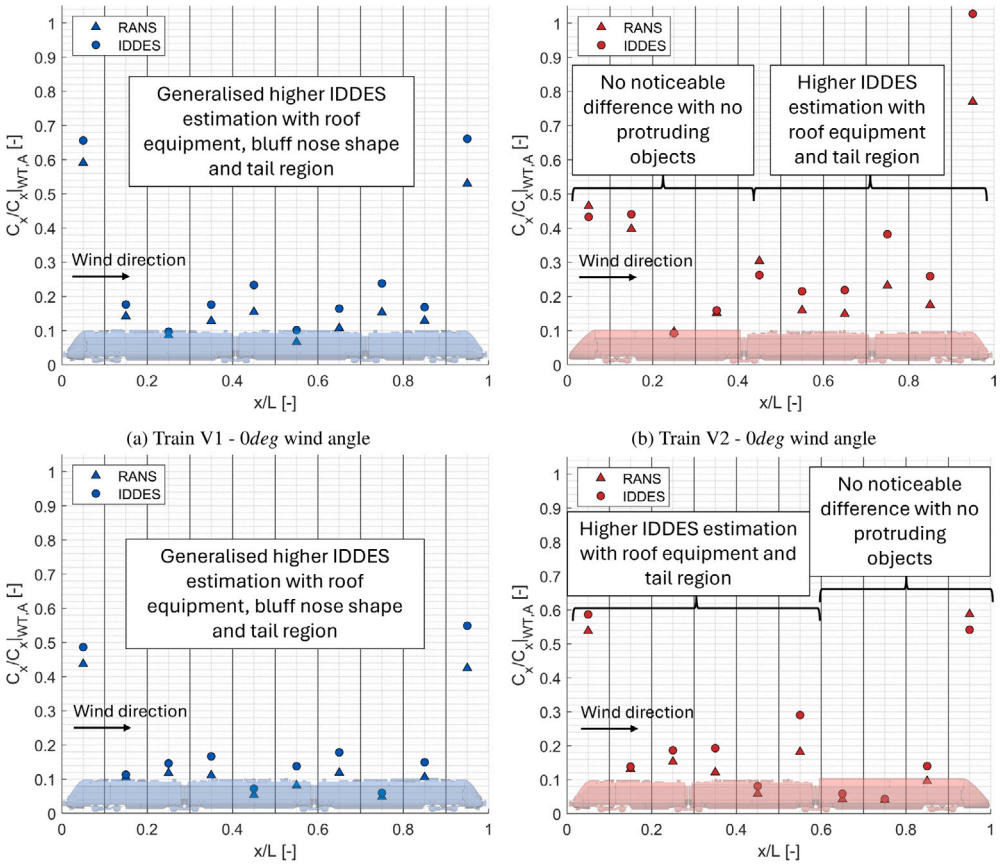

(a) Train V1 - 0*deg* wind angle

(b) Train V2 - 0*deg* wind angle

(c) Train V1 - 180*deg* wind angle

(d) Train V2 - 180*deg* wind angle

Fig. 6. C_x for sections normalised over the wind tunnel value of car A. Comparison between RANS and IDDES simulations.

In wake-dominated regions, the differences between RANS and IDDES are mainly related to the predicted wake recovery and pressure distribution in the near-wake region rather than to the overall wake extent. As shown by the velocity field on the roof slice of the train models Fig. 9, the IDDES simulations generally predict a faster wake recovery and higher streamwise velocities in the near-wake region compared to RANS, while the steady RANS simulations tend to produce a more diffused wake with lower velocity levels persisting farther downstream. Despite this faster wake recovery, the IDDES simulations are characterised by a slightly lower mean pressure coefficient in the tail region Fig. 7, which results in a marginally higher pressure drag contribution on the tail compared to RANS. However, as shown by the cumulative drag distribution Fig. 8, the drag increment associated with the tail region is comparable between the two approaches, indicating that wake-related effects play a secondary role in the overall drag discrepancy.

In regions characterised by strong geometric disturbances, such as roof-mounted equipment and bogies, the discrepancies between the two models are instead governed by near-wall flow behaviour. In steady RANS simulations, the flow in separated regions tends to be more stabilised, with lower wall shear stress and weaker pressure loads on windward surfaces. In contrast, the IDDES simulations resolve a more energetic near-wall flow, leading to higher wall shear stress and increased pressure levels on surfaces facing the incoming flow, as visible from Figs. 10 and 11. This behaviour is associated with a different separation and reattachment pattern, with IDDES predicting an earlier flow reattachment downstream of sharp edges.

Overall, the higher drag predicted by IDDES is the result of a combination of effects. While wake-related pressure differences at the tail contribute to a slightly higher local drag, the dominant contribution arises from increased pressure loads on geometrically complex components along the train, leading to a gradual and more pronounced increase of the cumulative drag. For streamlined geometries, where such near-wall and wake pressure effects are reduced, the predictions of the two modelling approaches show a closer agreement.

The results indicate that for the typical bluff-body or conventional geometry of a regional train (V1), the RANS model aligns reasonably well with wind tunnel results in estimating the aerodynamic drag of the leading car. However, it significantly underestimates the drag for the trailing car. In contrast, the IDDES model, while exhibiting larger errors for the leading car of V1, provides results that are more consistent with wind tunnel data, particularly in the tail region. For the modified train with a streamlined leading car (V2), the RANS model diverges considerably from the experimental values when the train is oriented at 0°. When the train is at 180°, with the streamlined car positioned at the tail, the RANS results show better agreement with wind tunnel data. IDDES simulations follow a similar trend but yield improved accuracy in the tail region compared to RANS.

In Fig. 6, the aerodynamic drag coefficient (C_x) of the train is divided into 10 sections along its length. As in previous comparisons, the C_x values for each section are normalised by the experimental mean value of C_x for car A. This representation provides a clear overview of the distribution of drag along the train and highlights the differences between the two numerical models.

In nearly every section, the IDDES results show higher C_x values compared to RANS. This discrepancy is particularly noticeable in regions with protruding elements such as bogies or roof-mounted equipment, where the increased turbulence and flow separation are better captured by the IDDES method. Conversely, in areas with streamlined geometries, such as car A in the V2 configuration, the results from the

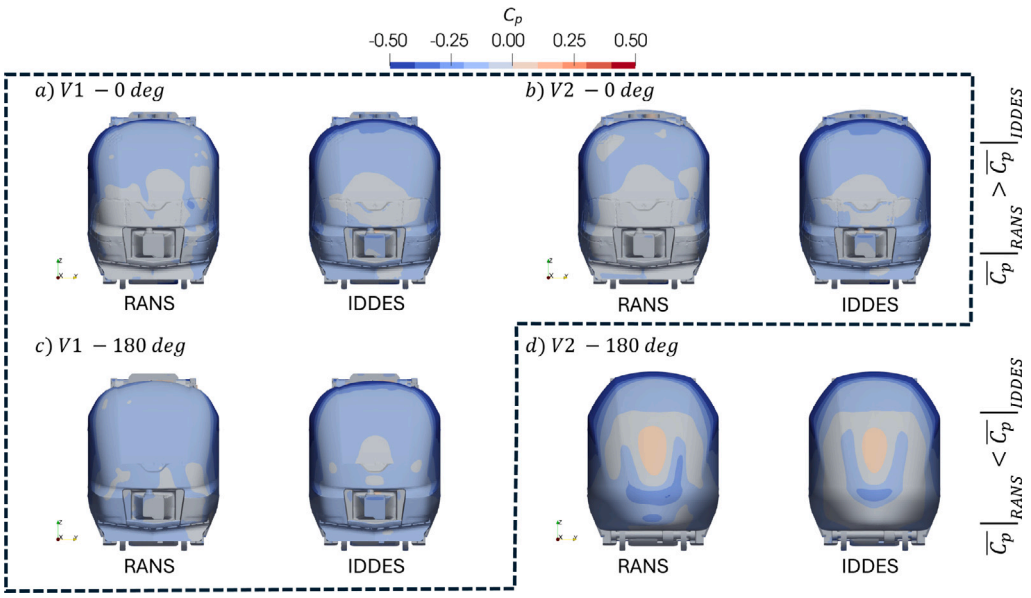

Fig. 7. Pressure coefficient over the tail of train models. Comparison between RANS and IDDES results.

two models are much closer, reflecting the reduced complexity of the flow in these regions.

In Fig. 7, the pressure coefficient distribution is reported for all the simulations considered. For configurations *a*, *b* and *c* the IDDES simulations present a stronger negative pressure compared to RANS. Conversely, for configuration *d*, IDDES presents higher pressure compared to RANS, coherently with the results reported in Fig. 6(d). This different behaviour can be attributed to the streamlined shape of car A, developing a different wake from the other bluff body coaches.

An additional observation, particularly evident for train V1 in Figs. 6(a) and 6(c), is the difference in the distribution of C_x between the head (first section) and tail (last section) of the train. In RANS simulations, the C_x values are lower at the tail compared to the head, consistent with the model's tendency to underpredict wake effects. In contrast, the IDDES simulations produce the opposite trend, with higher C_x values at the tail, showing the differences between the numerical models in capturing the wake dynamics and the associated aerodynamic loads.

The main conclusion is that RANS simulations might underestimate the drag evaluation compared to IDDES. This is particularly visible thanks to the drag computation of the trailing car and to the different results obtained when roof equipments are present. Such deviations between the two numerical models are not evident or smaller in case of streamlined bodies such as the head car of train V2.

To further support the analysis of the two numerical models, Fig. 8 shows the cumulative drag coefficient C_x, plotted along the length of the train models. As in the previous cases, the values of C_x are normalised by dividing by the experimental mean value of C_x for car A.

For configurations V1 (Figs. 8(a) and 8(c)), aside from the very initial section of the head car, the cumulative aerodynamic drag diverges significantly between the RANS and IDDES models. This divergence results in overall drag coefficients differing by approximately 22% of the IDDES simulation results.

In the case of configuration V2 at a 0-degree angle of attack (Fig. 8(b)), the initial section of the train model shows identical results for both numerical models. A similar pattern is observed for the 180-degree case (Fig. 8(d)), where the tail of the train model is streamlined. In this configuration, the cumulative drag does not differ significantly beyond the deviations accumulated in the head and middle sections of the model. Here, the discrepancy between the overall drag is reduced compared to train V1, but still in favour of IDDES that presents higher values of around 13%–16%.

For Figs. 6(b) and 8(d), it must be noted that differences between the two numerical models are exaggerated as they are normalised over the smaller value $C_x|_{WT,A}$ of the car A with streamlined shape.

Fig. 9 illustrates the non-dimensional velocity in the x-direction, defined as $U_{x,\mathrm{norm}} = |U_x/v|$, across planes normal to the z-direction that intersect the roof of the train models. The configurations at 180° for train models V1 and V2 are analysed using the two numerical approaches, RANS and IDDES.

For both train models, the roughness of the roof-mounted equipment introduces significant differences in the wake velocity profiles between the numerical models. Specifically, looking at the highlighted areas, IDDES predicts generally smaller wake regions compared to RANS, which leads to higher flow speeds in the wake area. This trend is particularly evident for train V1, where the tail's wake also exhibits this behaviour (Fig. 9(a)).

In contrast, for the more streamlined geometry of train V2 (Fig. 9(b)), the discrepancy between the two numerical models becomes almost negligible. This indicates that streamlined shapes are less sensitive to the modelling approach in terms of wake velocity prediction, as the flow remains attached for a larger portion of the geometry and generates less turbulence.

Fig. 10 shows the pressure coefficient and the skin-friction coefficient on the roof of the middle car of train V2 simulated at 180° using RANS and IDDES models. Both coefficients indicate that the RANS simulations predict a lower local flow velocity in the presence of roof-mounted equipment. As a consequence, the pressure coefficient predicted by IDDES is higher over surfaces characterised by sharp edges, while the skin-friction coefficient is generally higher, indicating a different flow reattachment position along the body surface and a different near-wall velocity gradient.

From a practical point of view, the RANS simulations tend to predict lower pressure values on surfaces facing the incoming flow, while the rear-facing surfaces are less strongly affected, as shown in Fig. 11. The higher pressure coefficient on the windward (positive-normal) faces is therefore identified as the main source of the discrepancy highlighted in the cumulative drag plot reported in Fig. 8. In simulations aimed at supporting train shape design, such features may mislead the designer, potentially leading to an underestimation of the contribution of these components to the overall aerodynamic drag. The adoption of smoother geometries, in addition to being beneficial for the final product, is also

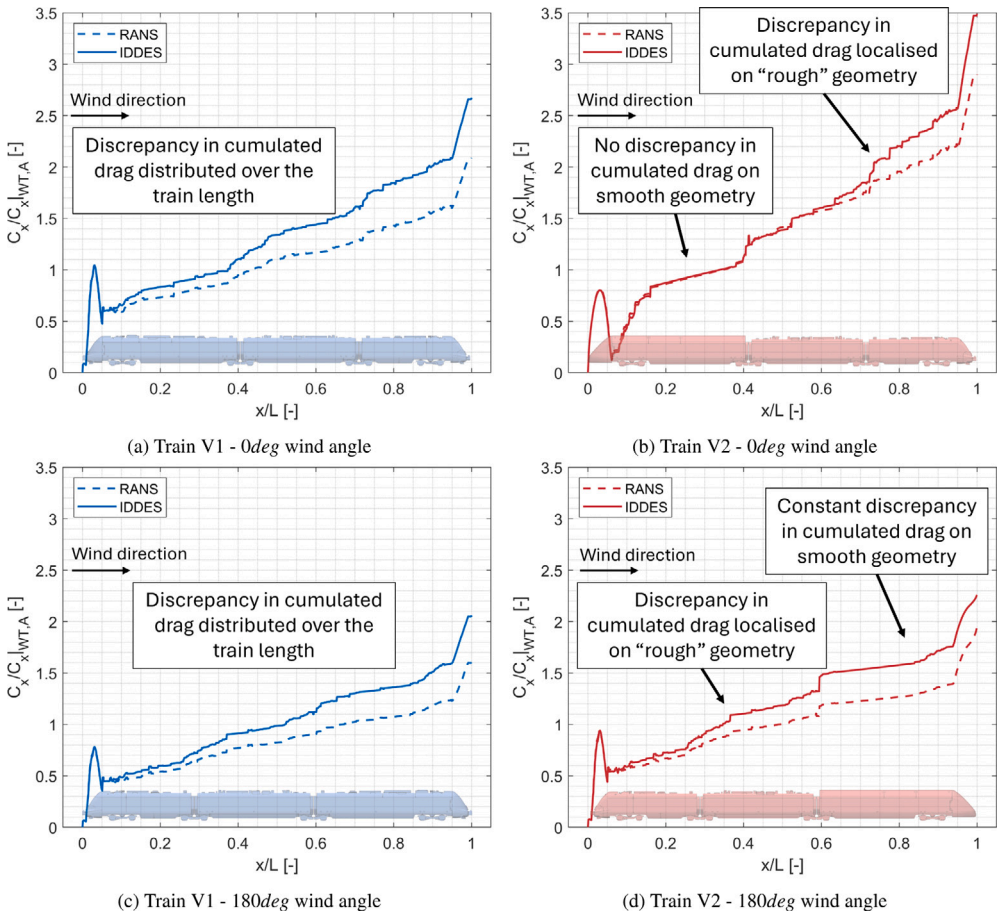

(a) Train V1 - 0*deg* wind angle

(b) Train V2 - 0*deg* wind angle

(c) Train V1 - 180*deg* wind angle

(d) Train V2 - 180*deg* wind angle

Fig. 8. Cumulative C_x normalised over the wind tunnel value of car A. Comparison between RANS and IDDES simulations.

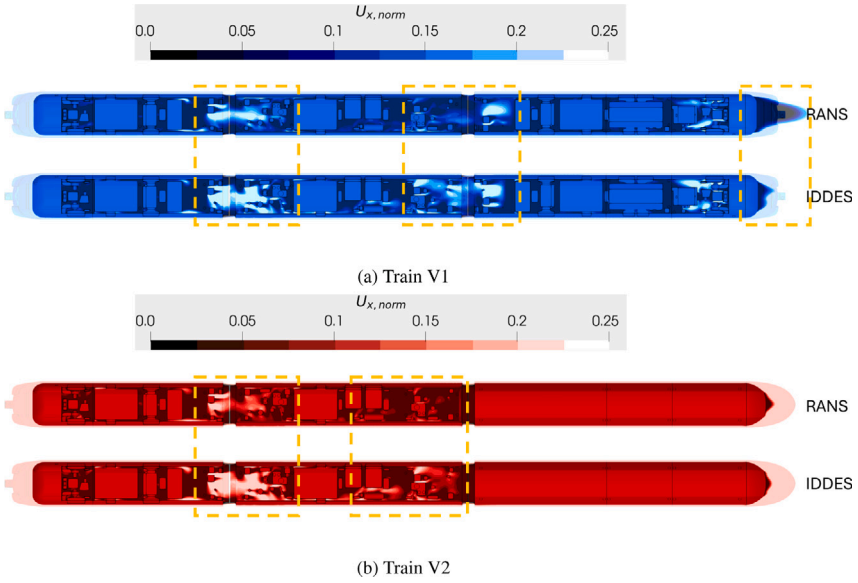

(a) Train V1

(b) Train V2

Fig. 9. Roof slice of the normalised flow speed in x direction for models at 180 deg. Comparison between RANS and IDDES.

expected to yield more consistent results between the two modelling approaches, as demonstrated by the streamlined head geometry of train V2 compared with train V1.

These conclusions are in agreement with other literature studies (Maleki et al., 2017; Zhang et al., 2023, 2022; Guilmineau et al., 2018). The results obtained highlight a limitation of the steady RANS CFD simulations. Indeed, RANS simulations risk underestimating the aerodynamic drag of complex train shapes, such as regional trains, particularly in regions near the tail and in areas where the turbulent wake region becomes more pronounced.

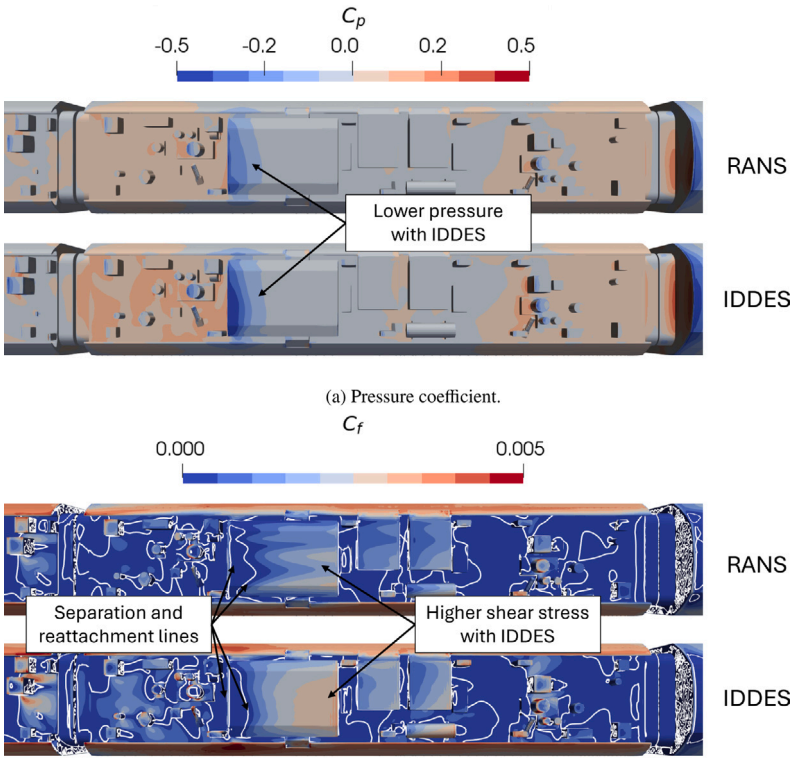

(a) Pressure coefficient.

(b) Skin friction coefficient with iso-curves $C_f = 0$.

Fig. 10. Roof view of the pressure and friction coefficients of middle car of the train model V2 at 180 deg. Comparison between RANS and IDDES.

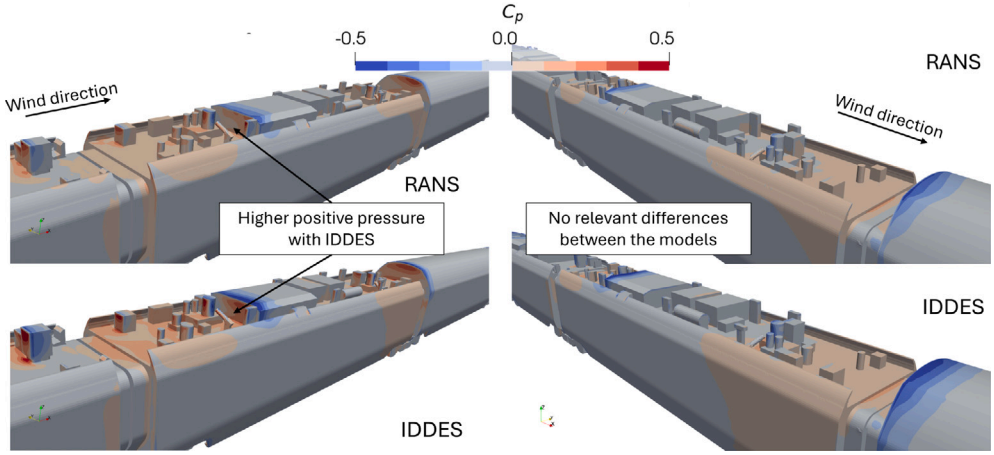

Fig. 11. Pressure coefficient of the middle car of train model V2 at 180 deg. Comparison of high pressure regions on the roof-mounted equipment between RANS and IDDES.

4. Conclusions

This research aims to identify the differences in simulating the aerodynamic drag of trains using the simplified method widely adopted in the industrial sector (RANS) and the state-of-the-art approach frequently employed in the railway field (IDDES). The numerical results are compared against wind tunnel data. The subject of the study is a regional train, with two configurations considered: a typical regional train and a modified version where the first car resembles a high-speed train. Since the train models are not symmetric in the longitudinal direction, tests were conducted at 0° and 180° angles of incidence to the wind to assess the effects of the different simulation approaches on the leading and trailing cars.

Compared to the available experimental data, both numerical models provide reasonable results. Notably, both models estimate values similar to the experimental ones in regions where the free flow impacts the body (the first car of the train model) and where the boundary layer begins to develop (the middle car of the train model). On the other hand, IDDES provides better results compared to RANS in regions where the flow separates from bluff bodies. This effect is less pronounced in the case of a streamlined body.

Overall, IDDES tends to predict higher aerodynamic drag than RANS in sections of the train where the geometry induces turbulent flows. These include the tail, bogies, and areas around roof-mounted auxiliary equipment, where the discrepancies between the two models are substantial. Conversely, for smoother geometries, the two numerical models produce similar results.

The two numerical methods, owing to their different approaches to turbulence modelling, estimate the aerodynamic drag of the train models with deviations ranging from 13% to 22% compared to the IDDES results, depending on the characteristics of the train's shape.

This study highlights the significant differences that can arise from employing different CFD models, particularly when analysing bluff geometries such as regional trains.

From a practical point of view, simulations based on RANS models are undoubtedly useful for manufacturers, as they are computationally efficient and generally provide valuable results with good to acceptable levels of accuracy. However, the limitations of these models must be carefully acknowledged. In particular, for geometries typical of regional trains, the present study indicates that RANS-based approaches may lead to an underestimation of the aerodynamic drag, failing to capture the full contribution to the overall resistance. Although IDDES simulations are, in most cases, still impractical for industrial applications due to their high computational cost, they are generally expected to provide more reliable estimates of aerodynamic drag.

Consequently, manufacturers may confidently rely on RANS simulations for head cars and streamlined geometries, whereas an increasing level of uncertainty should be expected as geometric complexity is introduced. When a highly accurate estimation of aerodynamic drag is required, and empirical correction factors are not deemed sufficient, higher-fidelity approaches such as IDDES are therefore recommended.

CRediT authorship contribution statement

Francesco Moro: Writing – original draft, Validation, Methodology, Investigation, Data curation. **Claudio Somaschini:** Writing – review & editing, Supervision, Methodology, Conceptualization. **Mikel Iraeta:** Writing – review & editing. **Daniele Rocchi:** Supervision, Project administration, Funding acquisition, Conceptualization.

Declaration of competing interest

The authors declare that they have no known competing financial interests or personal relationships that could have appeared to influence the work reported in this paper.

Acknowledgements

The authors acknowledge prof. Gisella Tomasini, Carlos Esteban Araya Reyes, Gonzalo Crespi and the technical staff of Politecnico di Milano wind tunnel for carrying out wind tunnel tests and proving the results. The authors are very grateful to CAF for allowing the use of technical data.

Data availability

The data that has been used is confidential.

References

Alšauskas, O., Teter, J., Triunfo, N., 2023. Tracking clean energy progress. URL: https://www.iea.org/energy-system/transport/rail.

Baker, C.J., 2014a. A review of train aerodynamics Part 1 - Fundamentals. Aeronaut. J. 118 (1201), 201–228. http://dx.doi.org/10.1017/S000192400000909X.

Baker, C.J., 2014b. A review of train aerodynamics Part 2 - Applications. Aeronaut. J. 118 (1202), 345–382. http://dx.doi.org/10.1017/S0001924000009179.

Baker, C.J., Brockie, N.J., 1991. Wind tunnel tests to obtain train aerodynamic drag coefficients: Reynolds number and ground simulation effects.

Baker, C., Johnson, T., Flynn, D., Hemida, H., Quinn, A., Soper, D., Sterling, M., 2019. Train aErodynamics: Fundamentals and Applications.

Brockie, N.J.W., Baker, C.J., 1990. The aerodynamic drag of high speed trains.

CEN, 2003. UNI EN 14067-2. Railway applications - Aerodynamics - Part 2: Aerodynamics on open track.

CEN, 2024. UNI EN 14067-4. Railway Applications - Aerodynamics - Part 4: Requirements and Test Procedures for Aerodynamics on Open Track.

Chen, G., Li, X.B., Liu, Z., Zhou, D., Wang, Z., Liang, X.F., Krajnovic, S., 2019. Dynamic analysis of the effect of nose length on train aerodynamic performance. J. Wind Eng. Ind. Aerodyn. 184, 198–208. http://dx.doi.org/10.1016/j.jweia.2018.11.021.

Flynn, D., Hemida, H., Soper, D., Baker, C., 2014. Detached-eddy simulation of the slipstream of an operational freight train. J. Wind Eng. Ind. Aerodyn. 132, 1–12. http://dx.doi.org/10.1016/j.jweia.2014.06.016.

Fujita, H., Sasaki, J., 2010. A Comparison Between Classical DES and DDES Using the In-House Computational Code. WSEAS Press.

Gao, G., Li, F., He, K., Wang, J., Zhang, J., Miao, X., 2019. Investigation of bogie positions on the aerodynamic drag and near wake structure of a high-speed train. J. Wind Eng. Ind. Aerodyn. 185, 41–53. http://dx.doi.org/10.1016/j.jweia.2018.10.012.

Gritskevich, M.S., Garbaruk, A.V., Schütze, J., Menter, F.R., 2012. Development of DDES and IDDES formulations for the k-ω shear stress transport model. Flow, Turbul. Combust. 88 (3), 431–449. http://dx.doi.org/10.1007/s10494-011-9378-4.

Guilmineau, E., Deng, G.B., Leroyer, A., Queutey, P., Visonneau, M., Wackers, J., 2018. Assessment of hybrid RANS-LES formulations for flow simulation around the Ahmed body. Comput. Fluids 176, 302–319. http://dx.doi.org/10.1016/j.compfluid.2017.01.005.

Guo, Z., Liu, T., Xia, Y., Liu, Z., 2022. Aerodynamic influence of the clearance under the cowcatcher of a high-speed train. J. Wind Eng. Ind. Aerodyn. 220, http://dx.doi.org/10.1016/j.jweia.2021.104844.

He, K., Su, X., Gao, G., Krajnović, S., 2022. Evaluation of LES, IDDES and URANS for prediction of flow around a streamlined high-speed train. J. Wind Eng. Ind. Aerodyn. 223, http://dx.doi.org/10.1016/j.jweia.2022.104952.

Heinz, S., 2020. A review of hybrid RANS-LES methods for turbulent flows: Concepts and applications. In: Progress in Aerospace Sciences. vol. 114, Elsevier Ltd, http://dx.doi.org/10.1016/j.paerosci.2019.100597.

Hemida, H., 2023. Contribution of computational wind engineering in train aerodynamics—past and future. J. Wind Eng. Ind. Aerodyn. 234, http://dx.doi.org/10.1016/j.jweia.2023.105352.

Huo, X., Liu, T., Chen, Z., Li, W., Gao, H., Wang, S., 2021. Comparative analysis of the aerodynamic characteristics on double-unit trains formed by different types of high-speed train. J. Wind Eng. Ind. Aerodyn. 217, http://dx.doi.org/10.1016/j.jweia.2021.104757.

IEA, 2019. The Future of Rail. IEA, URL: https://www.iea.org/reports/the-future-of-rail.

Kisielewicz, L., Tabbal, A., 1993. Validated computational aerodynamics for trains. J. Wind Eng. Ind. Aerodyn. 49 (1–3), 449–458. http://dx.doi.org/10.1016/0167-6105(93)90039-Q, URL: https://linkinghub.elsevier.com/retrieve/pii/016761059390039Q.

Li, X.B., Chen, G., Wang, Z., Xiong, X.H., Liang, X.F., Yin, J., 2019. Dynamic analysis of the flow fields around single- and double-unit trains. J. Wind Eng. Ind. Aerodyn. 188, 136–150. http://dx.doi.org/10.1016/j.jweia.2019.02.015.

Li, T., Hemida, H., Zhang, J., Rashidi, M., Flynn, D., 2018. Comparisons of shear stress transport and detached eddy simulations of the flow around trains. Trans. ASME J. Fluids Eng. 140 (11), http://dx.doi.org/10.1115/1.4040672.

Li, W., Liu, T., Martinez-Vazquez, P., Chen, Z., Huo, X., Liu, D., Xia, Y., 2022. Correlation tests on train aerodynamics between multiple wind tunnels. J. Wind Eng. Ind. Aerodyn. 229, http://dx.doi.org/10.1016/j.jweia.2022.105137.

Luo, C., Zhou, D., Chen, G., Krajnovic, S., Sheridan, J., 2020. Aerodynamic effects as a maglev train passes through a noise barrier. Flow Turbul. Combust. 105 (3), 761–785. http://dx.doi.org/10.1007/s10494-020-00162-w.

Maleki, S., Burton, D., Thompson, M.C., 2017. Assessment of various turbulence models (ELES, SAS, URANS and RANS) for predicting the aerodynamics of freight train container wagons. J. Wind Eng. Ind. Aerodyn. 170, 68–80. http://dx.doi.org/10.1016/j.jweia.2017.07.008.

Morden, J.A., Hemida, H., Baker, C.J., 2015. Comparison of RANS and detached eddy simulation results to wind-tunnel data for the surface pressures upon a class 43 high-speed train. Trans. ASME J. Fluids Eng. 137 (4), http://dx.doi.org/10.1115/1.4029261.

Moukalled, F., Mangani, L., Darwish, M., 2016. The Finite Volume Method in Computational Fluid Dynamics : An Advanced Introduction with OpenFOAM® and Matlab. In: Fluid Mechanics and its Applications, vol. 113, Springer, Cham, http://dx.doi.org/10.1007/978-3-319-16874-6, URL: https://link.springer.com/book/10.1007%2F978-3-319-16874-6#about.

Muñoz-Paniagua, J., García, J., 2020. Aerodynamic drag optimization of a high-speed train. J. Wind Eng. Ind. Aerodyn. 204, http://dx.doi.org/10.1016/j.jweia.2020.104215.

Niu, J., Zhou, D., Liu, F., Yuan, Y., 2018. Effect of train length on fluctuating aerodynamic pressure wave in tunnels and method for determining the amplitude of pressure wave on trains. Tunn. Undergr. Space Technol. 80, http://dx.doi.org/10.1016/j.tust.2018.07.031.

Orellano, A., Sperling, S., 2009. Aerodynamic improvements and associated energy demand reduction of trains. In: The Aerodynamics of Heavy Vehicles II: Trucks, Buses, and Trains. vol. 41, Springer Berlin Heidelberg, pp. 219–231. http://dx.doi.org/10.1007/978-3-540-85070-0{_}19, URL: http://link.springer.com/10.1007/978-3-540-85070-0_19.

Pope, S.B., 2000. Turbulent Flows. Cambridge University Press, Cambridge.

Shur, M.L., Spalart, P.R., Strelets, M.K., Travin, A.K., 2008. A hybrid RANS-LES approach with delayed-DES and wall-modelled LES capabilities. Int. J. Heat Fluid Flow 29 (6), 1638–1649. http://dx.doi.org/10.1016/j.ijheatfluidflow.2008.07.001.

Spalart, P.R., 2001. Young-Person's Guide Simulation Grids to Detached-Eddy. Technical Report, URL: http://www.sti.nasa.gov.

Spalart, P.R., 2009. Detached-eddy simulation. In: Annual Review of Fluid Mechanics. vol. 41, pp. 181–202. http://dx.doi.org/10.1146/annurev.fluid.010908.165130.

Spalart, P.R., 2021. Chapter four - hybrid RANS-LES methods. In: Durbin, P. (Ed.), Advanced Approaches in Turbulence. Elsevier, pp. 133–159. http://dx.doi.org/10.1016/B978-0-12-820774-1.00010-0, URL: https://www.sciencedirect.com/science/article/pii/B9780128207741000100.

Spalart, P.R., Deck, S., Shur, M.L., Squires, K.D., Strelets, M.K., Travin, A., 2006. A new version of detached-eddy simulation, resistant to ambiguous grid densities. Theor. Comput. Fluid Dyn. 20 (3), 181–195. http://dx.doi.org/10.1007/s00162-006-0015-0.

Spalart, P., Jou, W.-H., Strelets, M., Allmaras, S., 1997. Comments on the feasibility of LES for wings, and on a hybrid RANS/LES approach.

Sturt, R.A., Lynch, P.A., Burns, R.A., Clark, S.A., Horton, B.A., Derkowski, P.A., Keylin, A.T., Wilson, N.T., 2022. Aerodynamic Assessment and Mitigation – Design Considerations for High-Speed Rail. Technical Report, Federal Railroad Administration, URL: https://railroads.dot.gov/sites/fra.dot.gov/files/2024-05/Arup%20Aero-A%20Revision.pdf.

Tschepe, J., Nayeri, C.N., Paschereit, C.O., 2021. On the influence of Reynolds number and ground conditions on the scaling of the aerodynamic drag of trains. J. Wind Eng. Ind. Aerodyn. 213, http://dx.doi.org/10.1016/j.jweia.2021.104594.

Wang, S., Bell, J.R., Burton, D., Herbst, A.H., Sheridan, J., Thompson, M.C., 2017. The performance of different turbulence models (URANS, SAS and DES) for predicting high-speed train slipstream. J. Wind Eng. Ind. Aerodyn. 165, 46–57. http://dx.doi.org/10.1016/j.jweia.2017.03.001.

Wang, J., Minelli, G., Dong, T., Chen, G., Krajnović, S., 2019. The effect of bogie fairings on the slipstream and wake flow of a high-speed train. An IDDES study. J. Wind Eng. Ind. Aerodyn. 191, 183–202. http://dx.doi.org/10.1016/j.jweia.2019.06.010.

Wang, J., Minelli, G., Dong, T., He, K., Krajnović, S., 2020. Impact of the bogies and cavities on the aerodynamic behaviour of a high-speed train. An IDDES study. J. Wind Eng. Ind. Aerodyn. 207, http://dx.doi.org/10.1016/j.jweia.2020.104406.

Wang, S., Wang, R., Xia, Y., Sun, Z., You, L., Zhang, J., 2021. Multi-objective aerodynamic optimization of high-speed train heads based on the PDE parametric modeling. Struct. Multidiscip. Optim. 64 (3), 1285–1304. http://dx.doi.org/10.1007/s00158-021-02916-0.

Yang, W.C., Zhao, L., Deng, E., Ni, Y.Q., Zhao, W., Liu, Y.K., Ouyang, D.H., 2024. Spatial-temporal characteristics of the transient flow field around high-speed trains transiting the subgrade-cutting transition section under crosswinds. Alex. Eng. J. 86, 34–48. http://dx.doi.org/10.1016/j.aej.2023.11.042.

Yao, S.B., Guo, D.L., Sun, Z.X., Chen, D.W., Yang, G.W., 2016. Parametric design and optimization of high speed train nose. Optim. Eng. 17 (3), 605–630. http://dx.doi.org/10.1007/s11081-015-9298-6.

Zhang, J., Gidado, F., Adamu, A., He, K., Krajnović, S., Gao, G., 2023. Assessment of URANS, SAS, and IDDES on the bi-stable wake flow of a generic ship. Ocean Eng. 286, http://dx.doi.org/10.1016/j.oceaneng.2023.115625.

Zhang, J., Guo, Z., Han, S., Krajnović, S., Sheridan, J., Gao, G., 2022. An IDDES study of the near-wake flow topology of a simplified heavy vehicle. Transp. Saf. Environ. 4 (2), http://dx.doi.org/10.1093/tse/tdac015.

Zhang, J., Wang, J., Wang, Q., Xiong, X., Gao, G., 2018. A study of the influence of bogie cut outs' angles on the aerodynamic performance of a high-speed train. J. Wind Eng. Ind. Aerodyn. 175, 153–168. http://dx.doi.org/10.1016/j.jweia.2018.01.041.

Zhao, L., Zhang, Y.Q., Yang, W.C., He, H., Deng, E., 2026. Aerodynamic deterioration of high-speed trains passing through tunnel-bridge-tunnel transitions in canyon-ridge terrain under crosswind based on a parametric terrain model. Tunn. Undergr. Space Technol. 169, http://dx.doi.org/10.1016/j.tust.2025.107314.